Long-term alteration processes of iron fasteners extracted from archaeological shipwrecks aged in biologically active waterlogged media

Céline Rémazeilles, François Lévêque, Egle Conforto, Philippe Refait

Long-term alteration processes of iron fasteners extracted from archaeological shipwrecks aged in biologically active waterlogged media.

Céline Rémazeilles[a*], François Lévêque[b], Egle Conforto[a], Philippe Refait[a]

[a]LaSIE, Laboratory of Engineering Sciences for the Environment, UMR 7356 CNRS-University of La Rochelle, Avenue Michel Crépeau, F-17042 La Rochelle cedex 01, France

[b]LIENSs, Littoral, Environment and Societies, UMR 7266 CNRS-University of La Rochelle**,** 2 rue Olympe de Gouges, F-17000 La Rochelle, France.

corresponding author: Céline Rémazeilles, cremazei@univ-lr.fr

Abstract

Waterlogged woods and iron reinforcements extracted from archaeological shipwrecks were studied. The corrosion mechanisms of the reinforcements were investigated by analyzing the corrosion products using a multi-technique approach. The woods contained pyrite and greigite. The reinforcements showing different degradation states were corroded into siderite, chukanovite, mackinawite, pyrite and greigite. Then, two half-nails were soaked in neutral and acidic Na_2S solutions. Mackinawite precipitated only in neutral conditions. Through this study, the natural mackinawite-to-pyrite evolution process induced by a long-term exposure to sulfides is highlighted. This work also shows that iron sulfides can result from complex processes implying other sulfide-sensitive phases.

Keywords: archaeological shipwrecks / iron / sulfide-promoted alteration / iron sulfides / siderite

1. Introduction

Archaeological remains may contain marks testifying of crucial steps of long-term alteration processes. Thus, they represent very interesting systems to study for understanding the effects of a long-term exposure to harmful species. Through the analysis of iron fasteners extracted from archaeological shipwrecks, the present work deals with the effects on ferrous substrates of a long-term exposure to sulfides. The corrosion promoted by sulfides is an important issue for the durability of modern steel structures intended to be immersed or buried for a long time, such as nuclear waste storage containers for instance. In natural environments, sulfides can be provided by sulfide-producing microorganisms, fuels or minerals. In the case of archaeological wooden shipwrecks aged in aqueous and waterlogged media, conditions are favorable for anaerobic sulfide-producing bacteria to develop but also for their activity to be maintained for a very long time. Therefore, archaeological composite wood-iron assemblies extracted from waterlogged sites are perfect systems for understanding the effects, on ferrous metals, of a long-term exposure to sulfides by the study of corrosion product layers of the reinforcements. The contamination of wood by iron sulfides, a well known phenomenon and a major issue in the field of conservation of cultural heritage, is then attributed to the microbiologically influenced corrosion (MIC) of hundreds of nails used to assemble the boats wooden planks [1-3]. However, it can be mentioned that when MIC takes place, this occurs in addition to previous corrosion processes (aerated) but also in addition to other possible concomitant ones (e.g. promoted by chlorides or carbonates).

One of the first effects of MIC is the occurrence of FeS mackinawite [*e.g.* 4-12]. Depending on pH, hydrogen sulfide produced by anaerobic microorganisms, such as sulfate-reducing bacteria (SRB) bacteria, can dissociate into hydrosulfide ions HS^- and sulfide ions S^{2-} with $pKa_1 = 7.04$ and $pKa_2 = 11.96$ [13]. Therefore, in neutral or near-neutral conditions,

H_2S and/or HS^- react with Fe^{2+} ions resulting from the dissolution of the metal, leading to the precipitation of FeS at the surface according to reactions 1 and 2.

$$Fe^{2+} + H_2S \rightarrow FeS + 2H^+ \quad (1)$$

$$Fe^{2+} + HS^- \rightarrow FeS + H^+ \quad (2)$$

Nevertheless, the exposure to sulfides may not only promote corrosion but can induce subsequent transformations of previously formed corrosion products. As it happens, mackinawite is the first iron sulfide to precipitate in case of MIC but an exposure to sulfides can induce its transformation into greigite (Fe_3S_4), which can be in turn converted to pyrite (FeS_2) [14-17]. Besides, some iron (oxyhydr)oxides (α-FeOOH goethite, γ-FeOOH lepidocrocite, Fe_3O_4 magnetite, α-Fe_2O_3 hematite and ferrihydrite) are known to be sensitive to sulfides. It has been demonstrated that at 25°C, sulfides may promote the dissolution of a passive film and/or Fe(III) compounds previously formed on a steel surface through a multi-step reductive process. The nature of resulting products, i.e. dissolved species, colloidal or solid sulfates, sulfites, thiosulfates, polysulfides and sulfides (FeS and elemental sulfur), seem to depend on pH and sulfide concentration [18-21]. At last, Fe(II) carbonates proved to be reactive to sulfides as well. In neutral sulfide-containing solutions, synthetic and natural siderite ($FeCO_3$) and chukanovite ($Fe_2(OH)_2CO_3$) were converted to mackinawite owing to a dissolution-recrystallization mechanism, favored by the solubility of mackinawite, much lower than that of siderite or chukanovite [22-23]. This demonstrates that the effects of sulfides on a ferrous substrate are not restricted to the corrosion of the metal itself, as a long-term evolution process may involve successive transformations of corrosion products.

Previous works conducted by our team shown that mackinawite and greigite were detected in high amounts in woods of shipwrecks dated from the 18th and 19th centuries [24] and that greigite and pyrite were observed contaminating entirely two antic shipwrecks buried in waterlogged sediments [25,26]. In the present article, the evolution mechanisms of iron

corrosion products due to a long-term exposure to sulfides are thoroughly investigated. Nails extracted from three archaeological shipwrecks were analyzed and the results were compared to the previous studies [24-26]. This article deals specifically with the study of the iron reinforcements, while the study of the wood of two wrecks referred here has been already reported in [25]. Consequently, the first part starts by presenting detailed results of the third wreck. The three wrecks are dated from the period comprised between the 2nd and the 5th century AD, i.e. they can be considered to have aged along approximately the same time in their respective environments. Two wrecks were buried in anoxic waterlogged sediments while the third wreck remained lying on a riverbed. In addition, to elucidate the origin of significant differences observed between the nails of the various wrecks, a supplementary laboratory experiment was performed. Two halves of a same nail were immersed for 3 months in sulfide-containing solutions of different pH values. The main aim of this experiment was to assess the influence of pH on the possible transformation of previously formed iron sulfides and iron carbonates, and the formation of specific phases, in particular mackinawite FeS.

From all the obtained results, an overall process, including sulfide-sensitive corrosion products, is proposed.

2. Experimental

2.1 The archaeological perspective

The nails were extracted from three shipwrecks. Two of them were excavated from waterlogged sites and the third laid immersed in a river. It must then be emphasized that the environment of the third wreck, i.e. river water, is fundamentally different from that of the two other wrecks, i.e. anoxic waterlogged sediments.

The used artefacts were not subjected to any restoration treatment. More information, description and images of the objects from the wrecks of Mandirac and LSG4 can be found in previous publications [25-26]. A picture of the LSG4 wreck is also given in [26].

- The wreck of Mandirac (4^{th} century) was discovered in the site of Castelou/Mandirac corresponding to the ancient ports of Narbonne (France), now inland. In the course of an excavation program launched in 2010, the remains of a boat were found embedded in the dike [27-29]. A magnetic prospecting campaign conducted on site in 2014 revealed that the wood of this boat was abnormally magnetic throughout the entire wreck and that there was no more metal in the nails used for assembly. A plank was extracted during excavation and was studied to determine the origin of the magnetic signal. It was established that the magnetic properties of the wood were due to the presence of greigite and that the entire wreck was contaminated by greigite and pyrite assumed to result from the MIC of the iron fasteners [25]. The studied plank contained the rest of a nail, which was extracted and analyzed. The pH value of the wood surrounding the nail was equal to 3.3. This nail was then used for the laboratory experiment reported in this article (see section 2.2).

- LSG4 (2^{nd} century), for Lyon Saint-Georges wreck n°4, is one of the 16 wrecks excavated between 2002 and 2004 in a place intended for the building of an underground car park in the city of Lyon (France). This site corresponded to the ancient Saône riverbed [30]. The analysis of the wood revealed a high content of greigite and pyrite in the wreck probably due to the MIC of more than 2000 nails. In addition, magnetic measurement methods allowed detecting the presence of magnetite [25,26]. Two nails embedded in wood, still humid, were analyzed. The pH of the wood surrounding the nails was equal to 3.5. Both nails were entirely corroded, with no metal left, and presented a similar composition. The results obtained with one of them are reported in this article.

- The wreck of Courbiac (2^{nd}-5^{th} century), inventoried as the "wreck n°2 Courbiac-Saintes-Fontcouverte", is part of two Gallo-roman shipwrecks immersed at 7.5 m deep in the Charente river near Saintes (France) and excavated between 2015 and 2017 [31]. Part of the wrecks remained buried in the river sediment. However, the fragment of the hull timber provided for the study was extracted from a part outcropping the riverbed. The environment of these nails was then clearly different from that of the nails from Mandirac and LSG4, which remained in waterlogged sediments.

The considered fragment of the wreck of Courbiac is shown in Fig.1. It can be seen that it contained several nails showing an apparently good preservation state. A rapid non-destructive magnetic susceptibility measurement all along the wooden piece confirmed the presence of metal (α-Fe) in each nail. The nail pointed out by the black arrow was removed and analyzed. In addition, the analysis of the wood of this plank, not published elsewhere, is described in this article. The wood samples were extracted from the plank around the nail pointed out by the white arrow.

2.2 Sample preparation

The iron/wood samples were kept wet from excavation until analysis, wrapped in a plastic film in order to prevent their drying and preserve them from air, and kept at -20°C in a freezer. Freezing can damage the wood but it proved efficient to avoid the transformation of oxygen-sensitive mineral phases such as iron sulfides [32-35], which was our main concern.

- Preparation of wood samples: The procedure previously used for the wrecks of Mandirac and LSG 4 is thoroughly described in [25]. Concerning the hull timber fragment of the wreck of Courbiac, 14 wooden cubes of 1.9×1.9×1.9 cm^3 were cut using a ceramic blade in order to avoid any contamination of the samples by magnetic micro-particles possibly provided by a steel blade. Such contamination could influence further magnetic measurements.

- Preparation of nails: Immediately after their removal from the wood, the nails were embedded in epoxy resin. They were subsequently cut with a diamond wire saw in order to carry out analysis in cross sections. Nujol was used as lubricant in order to provide an oily film on the surface, so that oxygen sensitive phases were protected from air all along the cutting. To avoid any use of water, the sections were pre-polished in hexane with silicon carbide discs until grade 4000 (grain size of 5 μm). Then, non-aqueous diamond suspensions were used for polishing until grain size of 1 μm (DP Suspension A, Struers). If metal was still present, a metallographic observation was carried out on a cross-section with an optical microscope after a Nital (solution of 3 mL of HNO_3 in *q.s.* for 100 mL of ethanol) attack (about 30 s). The other cross-section was dedicated to the analysis of the corrosion product layers.

- Preparation of sulfide-containing solutions and nail to be immersed:

Two solutions were prepared with argon-deaerated water, by dissolution of sodium sulfide ($Na_2S.9H_2O$, purity higher than 98%, Sigma Aldrich) with a concentration $[S^{2-}] = 10^{-3}$ mol L^{-1}, sodium hydrogen carbonate ($NaHCO_3$, >99%, Fluka) with a concentration $[HCO_3^-] = 2 \times 10^{-3}$ mol L^{-1} and sodium chloride (NaCl, >99,5%, Sigma Aldrich) with a concentration $[Cl^-] = 0.015$ mol L^{-1}. The pH was adjusted using HCl to 7 for one solution and 3 for the other. These values are close to those measured on various wet archaeological woods contaminated by iron sulfides. Neutral pHs were observed for wrecks previously analyzed [24] and for the wreck of Courbiac (see further) while the pH values measured for the woods surrounding the nails of the wrecks of Mandirac and LSG4 were close to 3. Sodium hydrogen carbonate was added to the solutions to avoid a dissolution of the iron(II) carbonated solid phases due to the lack of carbonate species in solution.

Since the nail of the wreck of Mandirac was cut in the middle for analyzing the corrosion products (section 2.1), its two halves were used for the immersion in the sulfide-containing

solutions. It is important to note that only pyrite and siderite were detected in this nail before immersion. The immersion of the half-nails, the addition of Na_2S and the closure of the flask were realized as quickly as possible. The flasks were filled to the brim and hermetically closed.

2.3 Methods

- Analysis of mineral phases in the wood:

The methodology combines magnetic measurements methods allowing detection in the bulk and more classical surface analysis methods, namely Environmental Scanning Electron Microscopy coupled with Energy Dispersive Spectrometry (ESEM/EDS) and micro-Raman spectroscopy. The pH of the wood samples was also determined.

Magnetic measurements, i.e. susceptibility measurements and backfield acquisition of isothermal remanent magnetization (IRM) curves, were realized first. Secondly, ESEM/EDS, micro-Raman spectroscopy and surface pH measurements were carried out on slices cut from each cube. The cutting of slices was renewed for each surface analysis method and only the side corresponding to the inner part of the sample was analyzed, so that always a freshly cut surface unexposed to air was studied.

Magnetic susceptibility of wooden cubes (edges of 1.9 cm) was measured with a Kappabridge KLY4S (AGICO) device. Each cube was placed in a plastic cubic box of 8 cm^3 which was preliminarily used as a blank. The backfield isothermal remanent magnetization (IRM) curves were acquired with an initial magnetization in a 3T direct magnetic field and a progressive backfield produced by a pulse magnetizer (MMPM10, Magnetics Measurements). The magnetization was measured with a spinner magnetometer (JR6 Spinner, AGICO).

ESEM/EDS and micro-Raman spectroscopy analysis of wood samples was performed with the same procedures and instruments as for the analysis of the nails, which are described in

the next paragraph. Finally, the pH measurements were performed on wet wooden slices freshly cut from the samples with a surface electrode (Sentix Sur, WTW) calibrated using pH = 4.00 and pH = 7.00 buffer solutions (VWR).

- Characterization of the nails and their corrosion products:

The analytical procedure started with an optical microscope observation. The aim was to characterize the corrosion product layer morphology and to locate the zones of interest for microanalysis. Secondly, the identification of the corrosion products was achieved by combining ESEM/EDS and micro-Raman spectroscopy analysis. When metal was still present in the nails, as it was the case for the nails of the wreck of Courbiac, magnetic measurement methods were not applicable for characterizing magnetic corrosion products.

- ESEM/EDS and micro-Raman spectroscopy analysis

Electronic high-resolution micrographs and elemental compositions were obtained with a SEM microscope (FEI Quanta 200 FEG/ESEM) coupled with an EDAX Genesis EDS system for X-Ray microanalysis. Observations were performed in environmental mode, at low pressure (typically 0.002 atm) of water vapor, with an acceleration voltage of 20 kV. This experimental mode does not require preparation and is adequate for the analysis of non-conductive phases. Our preliminary tests proved that the water vapor surrounding the sample was not contributing to the EDS signal. To analyze iron sulfides present in a sample, EDS spectra were obtained focusing the electron beam on particles and the spectra were compared with a standard of pyrite.

Micro-Raman spectroscopy analysis was carried out with a Jobin Yvon High Resolution (HR LabRAM) spectrometer equipped with a microscope (Olympus BX41), a ×50 objective (long focal lens) and a Peltier-based cooled charge coupled device detector. The laser power was lowered down to 0.6 mW in order to prevent the transformation of heat-sensitive mineral phases. Spectra were recorded with the LabSpec software at a resolution of 0.2 cm^{-1}. The

samples were analyzed with an excitation wavelength of 632.82 nm. The duration of the analysis varied between 30 and 120 s depending on the analyzed compounds and the laser power used. The spot under the ×50 objective had a diameter of ~3 μm.

3 Results

3.1 Analysis of wood samples

The results of the analysis of the wood samples of the wreck of Courbiac are summarized in Fig. 2. Fig. 2a shows the backfield IRM curves of the 14 considered cubic wood samples. The red curve corresponds to the wood located just around a nail, i.e. to the wood sample that was the closest to the metal. This is the more magnetic sample with a single magnetic phase, of multi-domain grains of greigite. The curves at its right, in green color intensity scale, render a decrease of the greigite grain size. The presence of trace amounts of hematite cannot be excluded, which would explain the reddish color locally observed in the cracks of the wood. The curves at its left show the presence of two magnetic phases, greigite and magnetite that has a lower coercivity. It can be noticed that both phases have been detected only by magnetic measurement methods.

Micro-Raman spectroscopy experiments revealed the presence of pyrite in a few cubes, which was confirmed via the determination of the chemical composition by ESEM/EDS. Fig. 2b shows for instance an ESEM micrograph of framboïdal pyrite. Moreover, micro-Raman spectroscopy analysis revealed the presence of other phases, salts or sediments, namely sulfur α-S_8, gypsum ($CaSO_4 \cdot 2H_2O$), calcite ($CaCO_3$) and quartz (SiO_2) (Fig. 2c).

Surface pH measurements, performed on all cubic samples, revealed that the pH of the electrolyte impregnating the wood varied between 5.6 and 7.1. These values are significantly lower than that of 7.6 measured for the pH of the Charente River water.

3.2 Analysis of the nails

- Wreck of Courbiac (river water):

In the case of the wreck of Courbiac, the studied nail was not directly in contact with the wood of the hull. When it was extracted, it appeared that the nail had been imbedded in a wooden peg, shown by the arrow in Fig. 3a. It was assumed that this technique had been used for all nails of the wreck. The analysis started with a metallographic examination. The metal presented a heterogeneous microstructure with zones of ferrite (Fig. 3b) or acicular ferrite and perlite where some ferrite present a Widmanstätten structure (Fig. 3c) [36, 37]. This observation suggests different cooling rates during the manufacture of the object and a carbon content estimated between 0.1% and 0.3%. The corrosion product layers had a thickness of 1 to 2 millimeters (Fig. 3d) and highlighted a generalized carbonate-influenced corrosion process. They were composed mainly of carbonated Fe(II) phases, namely siderite and chukanovite (Fig. 3e), which are typical of corrosion processes occurring in deaerated conditions since dissolved O_2 would induce their transformation into Fe(III)-based compounds [38-40]. However, bright edges appeared within the carbonated corrosion products, as revealed by the ESEM micrograph of Fig. 3d (arrow 2). EDS microanalysis showed that these zones were rich in iron and sulfur (data not shown). Mackinawite and greigite were identified by Raman spectroscopy (Fig. 3e). At last, corrosion products were locally observed deep in the metal. Siderite, chukanovite as well as magnetite and Fe(II) hydroxychloride β-$Fe_2(OH)_3Cl$ were detected in the affected areas. The presence of β-$Fe_2(OH)_3Cl$ in more degraded zones of the metal suggested that the presence of chlorides in the river water induced a localized corrosion process. Similar conclusions were drawn for iron archeological artefacts extracted from anoxic soils, which presented locally β-$Fe_2(OH)_3Cl$ in the corrosion product layers [41]. The impact of chlorides is not specifically discussed in this article because it was considered as a corrosion process not associated with sulfide species.

- Wrecks of Mandirac and LSG4 (waterlogged sediments):

Fig. 4 displays cross section, ESEM micrograph in chemical contrast and EDS spectra of a nail extracted from the wreck of Mandirac. It must be compared with Fig. 5 that deals with a block nail extracted from LSG4. The cross section of both nails revealed that there was no more metal (Figs. 4a and 5a). On the ESEM micrographs, bright zones (label 1 in Figs. 4b and 5b) and dark zones (label 2 in Figs. 4b and 5b) could be observed. They correspond respectively to sulfur-rich and sulfur-poor zones (Figs. 4c and 5c). It was subsequently demonstrated by micro-Raman spectroscopy that the bright zones were composed of pyrite and that the dark zones were composed of siderite (spectra not shown). Both nails presented the same corrosion products but their distribution was different. As observed in Fig. 4b for the nail of the wreck of Mandirac, pyrite was heterogeneously distributed in a porous matrix composed of siderite. Moreover, weak peaks of marcasite (FeS_2) appeared on a few Raman spectra with those of pyrite. For the nail of LSG4, Fig. 5b shows an advanced pyritization of the block with wood cells completely filled with pyrite. However, siderite cores of different sizes remained disseminated in the block, including the central one delineated by dashes in Fig. 5a, which was the biggest. A detail of a small one is presented in Fig. 6. The corresponding ESEM micrograph shows a border of intermediate chemical contrast between a dark and a bright zone (Fig. 6a). Siderite and pyrite were identified by micro-Raman spectroscopy in the dark and bright zones respectively (spectra 1 and 3 in Fig. 6b) and the spectrum of the border shows the two bands of pyrite at 345 cm^{-1} and 380 cm^{-1} (spectrum 2 in Fig. 6b). However, these bands seem to be superimposed to a larger band centered at 360 cm^{-1}, which can be attributed to greigite. The latter is characterized by two partially overlapping bands at 350 cm^{-1} and 365 cm^{-1} [17]. This border was sometimes observed at the interface between siderite and pyrite for the nail of LSG4 but not for the nail from the wreck of Mandirac.

3.3 Immersion in sulfide-containing solutions of various pH values

The aim of this laboratory experiment was to study the possible transformation of pre-existing iron carbonates and the influence of pH on this transformation. The results described here are focused on the identification of products to assess the influence of pH on the occurrence of sulfide-containing compounds. Images of the half-nails immersed in their sulfide-containing solutions are shown in Fig. 7. Fig. 7a and 7a' correspond to the half-nail immersed in the neutral solution and Fig. 7b and 7b' correspond to the half-nail immersed in the acidic solution.

As shown in Fig. 7a, a black suspension appeared in the neutral solution after one day of immersion and a black precipitate progressively accumulated in the bottom of the flask. The nature of the black precipitate was determined by micro-Raman spectroscopy, after three months of immersion (Fig. 7a'). The corresponding Raman spectrum is characterized by peaks at 178, 263, 319, 329 and 365 cm^{-1}, which corresponds to Fe(III)-containing (i.e. partially oxidized) mackinawite $Fe^{II}_{1-3x}Fe^{III}_{2x}S$ [17,42]. This compound is mainly characterized by the sharp Raman peaks at about 178, 263, 319 and 329 cm^{-1} that do not relate to any other Fe-S phase. However, as reported in previous studies [17,42], an additional shoulder is seen on the high wavenumber side of the peak at 329 cm^{-1}, located in the present case at 365 cm^{-1}. This position also corresponds to the main Raman peak of greigite. Actually, Fe(III)-containing mackinawite is a transient compound formed during the transformation of mackinawite to greigite and it is still not clear whether the shoulder at 365 cm^{-1} is indeed associated with this compound or due to a small amount of greigite. In any case, when such a spectrum is obtained, the formation of greigite as a minor phase cannot be discarded. The surface of the half-nail was analyzed after immersion and the corresponding Raman spectrum is displayed in Fig. 7a'. This shows the bands of Fe(III)-containing mackinawite, as described

above, and peaks of pyrite at 330 and 383 cm^{-1}. However, siderite with the main peak expected at 1085 cm^{-1} was not detected supporting its sensitivity to sulfides and its transformation into mackinawite.

For the half-nail immersed in the acidic solution, the results were different. No black precipitate appeared but the solution became trouble. After three months, the flask was reopened and the half-nail was removed (Fig. 7b). The surface was attacked and presented numerous cracks and a micro-Raman spectroscopy analysis revealed a mixture of pyrite and elemental sulfur α-S_8 (spectrum 1 in Fig. 7b'). The particles present in suspension and responsible for the turbidity of the solution were filtered. They corresponded to elemental sulfur (spectrum 2 in Fig. 7b'). Siderite was not detected at the surface of the half-nail. Afterwards, the pH of the remaining solution was raised by a dropwise addition of a 0.1 M NaOH solution in order to provoke iron precipitation. When the solution became black, the suspension was filtered and the solid was analyzed by micro-Raman spectroscopy. It corresponded to magnetite Fe_3O_4 (Fig 7b' spectrum 3). The absence of siderite in the half-nail and the precipitation of magnetite in the solution demonstrated that the immersion of the sample induced a dissolution of siderite. However, the pH was too low for mackinawite to precipitate since a pH close to 3 represents the limit of solubility of FeS at ambient temperature [43-44]. The precipitation of sulfides into elemental sulfur could be due to a slight oxidation of the solution [18]. Consequently, for the half-nail in the acidic solution, the dissolution of siderite resulted rather from the low pH than to the exposure to sulfides. This demonstrates that mackinawite, which was detected neither in the nail of the wreck of Mandirac nor in the nails of LSG4, could not be present because these nails were surrounded by acidic electrolytes inside the shipwreck. Moreover, mackinawite had not been detected inside the wood of both wrecks, even when pH was measured higher than 3 [26].

4. Discussion

4.1. Formation and evolution of iron sulfides in the wood and at the surface of the nails

The archaeological shipwrecks represent iron-reinforced structures, which naturally aged in aqueous and waterlogged media. The anoxic conditions of burial and the abundance of organic matter are particularly favorable for the development of sulfide-producing bacteria and the observed iron sulfides can be considered to result from microbiological activity. The formation and evolution processes of the iron sulfides may however differ whether these compounds are located close to the nails, and thus somehow associated with the corrosion process of the nails, or present in the wood far from the nails. Both cases are discussed in this section, that of the wood first, that of the nails second.

The analysis of the samples from the wreck of Courbiac demonstrated that greigite and pyrite were present inside the wood. These compounds are the same as those detected in the wood of the wrecks of Mandirac and LSG4 [25]. The three wrecks are dated from Antiquity and contain the same iron sulfides, while the wood of more recent wrecks (19^{th} and 18^{th} c.) contains mackinawite and greigite [24]. These three iron sulfides are involved in an evolution process that has already been studied through laboratory experiments. It was demonstrated that mackinawite was transformed to pyrite via greigite [16,17,42]. This transformation process begins with an *in situ* oxidation of $Fe^{II}S$ mackinawite that leads in a first step to Fe(III)-containing mackinawite ($Fe^{II}_{1-3x}Fe^{III}_{2x}S$) [17-42]. The crystal structure of mackinawite may be able to withstand up to 20% Fe(III) [45], thus corresponding to a maximal *x* value of 0.11. For higher oxidation rates, i.e. for a higher proportion of Fe(III), a solid state transformation occurs [46], leading to greigite, which contains 66.7% of Fe(III) (Fe_3S_4 is actually $Fe^{II}Fe^{III}_2S_4$). The last step is the transformation of greigite into pyrite. It does not correspond to a subsequent oxidation of the remaining Fe(II) but implies the reduction of Fe(III) to Fe(II) and the oxidation of $S(-II)^{2-}$ sulfide ions to $S(-I)_2^{2-}$ disulfide ions [14]. The

entire reaction mechanism can be written as follows, with HS^- being considered both as the oxidant and as the sulfide supplier in neutral and near neutral conditions (reactions 3 to 5):

$$(1\text{-}x)Fe^{II}S + xHS^- \rightarrow Fe^{II}_{1-3x}Fe^{III}_{2x}S + 2xe^- + xH^+ \quad (3)$$

$$\left(\frac{3}{1-x}\right)Fe^{II}_{1-3x}Fe^{III}_{2x}S + \left(1-\frac{3x}{1-x}\right)HS^- \rightarrow Fe_3S_4 + \left(2-\frac{6x}{1-x}\right)e^- + \left(1-\frac{3x}{1-x}\right)H^+ \quad (4)$$

$$Fe_3S_4 + 2HS^- \rightarrow 3FeS_2 + 4e^- + 2H^+ \quad (5)$$

For the mackinawite-to-pyrite evolution process to be completely achieved, a sufficient supply of sulfides is necessary. In natural environments, this may take a long time. The age of wrecks is then interesting to consider because it allows, even empirically, estimating an apparent duration of exposure to sulfides, at the scale of a few or of several tens of centuries. Consequently, the study of several remains dated from several ages and extracted from waterlogged media is likely to provide a relevant illustration of the long-term effects of an exposure to sulfides on iron substrates and of the mackinawite-to-pyrite natural evolution process, each wreck being representative of a given step. The combination of the study carried out on antic wrecks (the present article and [25]) and of a previous study carried out on more recent wrecks (i.e. 19th and 18th c. [24]) constitutes a remarkable demonstration of the whole process through the detected iron sulfides in each of them. Thus, the more recent wrecks fit with the mackinawite-to-greigite step (reactions 3 and 4) and the antic wrecks fit with the greigite-to-pyrite step (reaction 5). Moreover, greigite was detected in ancient and recent wrecks as well, corroborating its intermediate role in the process. Mackinawite was not detected in the antic wrecks but this phase probably formed during the early stages of the burial, when anoxic conditions established, and is now completely transformed.

The analysis of the corroded nails (or remains of nails) demonstrated that the iron reinforcements could be in very different degradation states for wrecks of similar ages (Figs. 3 to 5). The nail of the wreck of Courbiac was weakly corroded compared to the nails of the wrecks of Mandirac and LSG4, the metal of whose had completely disappeared. Moreover, if

the nature of iron sulfides inside the wood was the same for the three wrecks (i.e. greigite and pyrite), the iron sulfides detected in the nails were not always similar to those detected in the wood they were extracted from. Indeed, the corrosion product layer of the nail of the wreck of Courbiac contained a small amount of mackinawite and greigite, while those of the wrecks of Mandirac and LSG4 showed a high amount of pyrite. In the nail of LSG4, greigite was also detected in an intermediate border separating siderite and pyrite zones, shown in Fig. 6. Besides, the observation of the corrosion patterns highlighted some similar features between nails but also differences. The nail of the wreck of Courbiac and the nail of LSG4 showed that iron sulfides were located in the outer part of the corrosion product layer, the inner part being composed of siderite and/or chukanovite.

In particular, the nail of the wreck of Courbiac showed that iron sulfides were located at the interface between the inner part of the corrosion product layer and the wooden peg initially surrounding the nail (Fig. 3). Compared to the nails of the wrecks of Mandirac and LSG4 (Figs. 4 and 5), this nail was the only one where metal remained. Grousset et al. [47] reported a comparable pattern for nails of the shipwreck Arles Rhône 3, dated from the Gallo-Roman period and extracted from the Rhône River. Those nails still contained metal too and were covered with a corrosion product layer mainly composed of carbonated corrosion products (i.e. siderite and chukanovite). Mackinawite and greigite were identified in the outer part of this layer. Around the nails, the wood has solidified and its cells were filled with pyrite [47]. Therefore, in the case of the nails of the wrecks of Courbiac and Arles Rhône 3, iron sulfides were not in contact with the metal. It can then be proposed that their occurrence was not directly linked to the corrosion of the metal substrate, but resulted from the subsequent transformation of previously formed corrosion products, as discussed in section 4.2.

The corrosion pattern of the nails of the wreck of Mandirac was different from the others, showing no stratification, but a heterogeneous repartition of pyrite inside a matrix made of

siderite (Fig. 4a). Due to different morphologies observed on the studied nails, two significant types of corrosion patterns were schematized in Fig. 8. Type A represents the nail of the wreck of Courbiac. The corrosion pattern of the nails of Arles Rhône 3, as described in [47], can be associated with it. It is characterized by a weakly corroded substrate and a predominance of carbonated corrosion products, while iron sulfides are present as thin borders in the outer part of the corrosion system. Type B represents the nails of the wreck of Mandirac and LSG4. It is characterized by an association of siderite and pyrite (including possible traces of greigite) with different arrangements of both phases.

Our results suggest that the nature of iron sulfides present in the corrosion systems of the reinforcements (including Arles Rhône 3) could be related to the degradation states of the metal substrate. Mackinawite and greigite were found on the least degraded nails (wrecks of Courbiac and Arles Rhone 3 [47], while pyrite (and greigite locally) were found on the most degraded nails (wrecks of Mandirac and LGS4). As previously emphasized, all wrecks (including Arles Rhône 3) were dated from the same period and the iron sulfides present in the woods were the same, suggesting that the respective durations of sulfide exposure of the remains could be comparable. However, the wreck of Courbiac and Arles Rhône 3 were extracted from a river while the wrecks of Mandirac and LSG4 were excavated from compact waterlogged sediments. Thus, the burial medium appears to be a relevant parameter explaining the observed differences. For instance, the wreck of Courbiac was excavated at about 7.5 meters under water and the extracted fragment (Fig. 1) was not buried in the sediments so was not subjected to anoxic conditions, at least in the later stages of ageing. However, the presence of iron sulfides testified for a sulfide-producing activity, which occurred certainly locally, in confined and deaerated areas inside the wood and closed to the reinforcements where a few anaerobic bacterial colonies could develop. On the contrary, the wreck of Mandirac and LSG4 aged in anoxic environments, much more favorable for an

intense anaerobic bacterial activity. Consequently, the more the conditions are anoxic and favorable for SRB development, the more the mackinawite-to-pyrite transformation process is advanced.

The burial conditions could then have an impact on the kinetics of the mackinawite-to-pyrite conversion process due to the intensity of the sulfide-producing activity they implied. The nails of the wrecks of Courbiac and Arles Rhône 3 are then characteristic of the mackinawite-to-greigite transformation step due to a poor bacterial activity implied by the immersion context. Those of the wrecks of Mandirac and LSG4 are characteristic of the greigite-to-pyrite step due to an intense bacterial activity favored by a general anoxic feature of the burial context. In addition here also, mackinawite certainly formed on the reinforcements of the wrecks of Mandirac and LSG4 during the early stage of the burial in the sediments, but is now completely transformed.

4.2. Formation of iron sulfides from previously existing iron carbonates and possible evolutions of the corrosion system

As previously mentioned, the iron sulfides were mainly located in the external part of the corrosion products layers of the nails or rests of nails. This is apparently in contradiction with a true MIC process where bacterial activity at the vicinity of the metal involves an interaction between sulfide species and metal surface and thus the formation of iron sulfides on the metal surface. As described in Fig. 8, the corrosion product layers were composed of an important amount of carbonated corrosion products (siderite and chukanovite). These compounds constituted the inner part of the layer (in contact with the metal) and were predominant for the less degraded nails (wrecks of Courbiac and Arles Rhône 3 [47]). This means that iron carbonates were probably more exposed to sulfides than the metal itself. The experiment described in part 3.3 (Fig. 7a and 7a') and previous works demonstrated the sulfide-sensitivity

of carbonated corrosion products [21-23]. In sulfide-containing neutral or near-neutral conditions, siderite and chukanovite are converted to mackinawite. The reactions 4 for siderite and 5 for chukanovite more likely involve dissolution-precipitation processes and can be written as:

$$FeCO_3 + HS^- \rightarrow FeS + HCO_3^- \quad (4)$$

$$Fe_2(OH)_2CO_3 + 2HS^- \rightarrow 2FeS + CO_3^{2-} + 2H_2O \quad (5)$$

Consequently, the presence of iron sulfides can be explained here by the transformation of iron carbonates, which raises the question of the real contribution of sulfides species to the corrosion of the metal in the studied system. Indeed, the mackinawite-to-pyrite evolution process induced by a prolonged exposure to sulfides is possible whatever the mechanism initially leading to mackinawite.

The concomitant presence of iron carbonates and iron sulfides in the corrosion product layers suggests in fact a long-term mixed alteration process, influenced by both carbonates and sulfides. The contribution of carbonates could be balanced by the sulfide-producing activity of bacteria. For instance, in the wood of the wreck of Courbiac, pyrite was only scarcely observed in a few wooden cubes. Magnetic methods detected also magnetite suggesting that iron scattered inside the wood was in excess towards sulfides, because the conditions were not favorable for sulfide-producing bacteria development. So, even if the presence and accumulation of Fe(II) carbonated phases prove that anoxic conditions were met at the vicinity of the metal surface, it can be assumed that the corrosion process was not promoted by sulfides in this case. The iron present in iron sulfides observed here and there inside the wood could be environmental or provided by the purely electrochemical corrosion of the reinforcements as well. The same analysis can be applied to the nails of the wreck Arles Rhône 3 [47]. On the contrary, the other nails from the wrecks of Mandirac and LSG4 contained a much higher proportion of pyrite. Since these artefacts had no metal left and

showed different corrosion patterns, it is difficult to estimate the contribution of MIC and the produced sulfide species in the whole corrosion process but it was probably much more important. Besides, the presumed high sulfide production rate implied by the sedimentary burial context could accelerate the kinetics of the siderite-to-mackinawite transformation and then the subsequent mackinawite-to-pyrite transformation process. The final product of this process, i.e. pyrite, could then be obtained for the nails of the wrecks of Mandirac and LSG4. The process could not be activated by a constant high sulfide production rate in the case of the nails of the wreck of Courbiac and Arles Rhône 3 so that it only led to greigite after the siderite-to-mackinawite transformation step.

As discussed above, the presence of iron sulfides in the corrosion product layers can result from a complex anoxic process composed of a combination of sub-processes represented in Fig. 9 and corresponding to a succession of alteration products leading to a final system. Two sub-processes are proposed starting from the corrosion of the metal, assuming that corrosion can be promoted by sulfides or not, depending on the intensity of the sulfide-producing activity of bacteria. The sub-process starting by MIC, inducing the formation of mackinawite as a corrosion product of the metal and leading to pyrite as the final compound, is a process entirely influenced by sulfide species. In contrast, when iron sulfides result from the transformation of sulfide-sensitive corrosion products, such as siderite and chukanovite, the process is only partially influenced by sulfide species because the metal itself does not interact with these species. The Type A corrosion pattern (see dots in Fig. 9) seems representative of this scenario.

Once the sulfide-producing activity becomes sufficiently important, both sub-processes are likely to occur simultaneously on a same substrate and pyrite should be the final product in any case. However, a mixture of siderite and pyrite was observed for the nails of the wrecks of Mandirac and LSG4. The overall evolution process would then be in this case the siderite-

to-pyrite transformation that involves mackinawite and greigite as intermediate transient phases. Greigite was scarcely detected as displayed in Fig. 6 but mackinawite was not detected at all. This phase is crucial and its absence suggests that the transformation of siderite to mackinawite no longer occurs. This could be due to a progressive drop of the pH all along the burial. Indeed, the experiment consisting in the immersion of the half-nail of the wreck of Mandirac in the acidic solution did not lead to the precipitation of mackinawite (Fig. 7b). The pH of the wood surrounding the studied artefacts from the wreck of Mandirac and LSG4 was measured around 3. This value corresponds to the limit of solubility of mackinawite. Therefore, even if iron carbonates are still present, their transformation into mackinawite is not possible anymore when the conditions become too acidic for mackinawite to precipitate. However, the transformation of greigite into pyrite remains possible if sulfide species are still supplied, leading to a two-phase siderite + pyrite system, as observed on Type B (see dots in Fig. 9). This two-phase system is probably the final result of the long-term alteration process of the reinforcements and could be reached a long time after the complete consumption of the metal.

5. Conclusion

Greigite and pyrite were detected in the wood of three archaeological shipwrecks dated from Antiquity and excavated from two different waterlogged media (soil, riverbed). Coupled to previous studies, which showed the presence of mackinawite and greigite in the wood of other archaeological shipwrecks, a link could be made between the nature of iron sulfides and a short- *vs* long-term exposure of artefacts to sulfides. This link is based on the mackinawite-to-pyrite evolution process, which was already demonstrated via laboratory experiments but is remarkably illustrated here by naturally aged systems.

In all cases, the extracted reinforcements (iron nails) were corroded into iron (hydroxy)carbonates (i.e. siderite and chukanovite) and iron sulfides (i.e. mackinawite, greigite and pyrite) but the degradation states and the amount of iron sulfides in the corrosion product layers were very different and depended on the burial context. Two types of long-term corrosion patterns were distinguished:

-Type A: the reinforcements are weakly corroded with a predominance of carbonated corrosion products and a low amount of iron sulfides located in the outer part of the corrosion system. This pattern is typical of remains extracted from riverbeds.

-Type B: the reinforcements do not contain metal anymore. The remaining artefacts are only composed of siderite and pyrite (including traces of greigite). This pattern is typical of remains excavated from anoxic waterlogged soils.

Type A highlighted the fact that, even in a context of iron corrosion, the presence of iron sulfide is not necessarily due to MIC process, associated with sulfide-producing bacteria, of the metal substrate. The presence of sulfide-sensitive phases, such as siderite and chukanovite, constitutes a possible route to produce mackinawite and then to initiate a mackinawite-to-pyrite transformation process, in parallel of the process possibly induced by MIC.

Thus, the final configuration of the system altered by a long-term exposure to sulfides, probably reached after the metal is completely consumed, would theoretically consist in only pyrite. However, a progressive decrease of the pH over time could prevent the transformation of siderite to mackinawite and induce a final two-phase system composed of siderite and pyrite, as observed for type B.

Acknowledgements

The authors are grateful to archaeologists, restorers and researchers who provided the samples and would like to associate them to this work.

Jonathan Letuppe (EVEHA and UMR-5607 AUSONIUS CNRS / Bordeaux Montaigne University) is warmly thanked for providing the sample of the wreck n°2 Courbiac-Saintes-Fontcouverte.

Many thanks are addressed to Corinne Sanchez (Archeology of Mediterranean Societies, UMR-5140 CNRS / University of Montpellier 3 / Ministry of Culture and Communication / Labex Archimedes) and Marie-Pierre Jézégou (DRASSM) for letting us bringing the plank from the wreck of Mandirac.

Laure Meunier and Marine Crouzet (Arc-Nucléart) are also warmly thanked for providing the nails of the wreck LSG4.

The authors also thank Nicolas Plasson, Maylis Minjacq, Antoine Trosseau (students) and Guillaume Lotte (LaSIE) for their contribution to analysis.

Data Availability

The raw/processed data required to reproduce these findings cannot be shared at this time due to legal or ethical reasons.

References

[1] I.D. Mac Leod and C. Kenna, Degradation of Archaeological Timbers by Pyrite: Oxidation of Iron and Sulphur Species. In: P. Hoffmann, (Ed.) Proceedings of the 4th ICOM Group on Wet Organic Archaeological Materials Conference, Bemerhaven, 1990, 133-141.

[2] M. Sandström, F. Jalilehvand, I. Persson, U. Gelius and P. Frank, Acidity and Salt Precipitation on the *Vasa;* The Sulfur Problem. In: P. Hoffmann, J.-A. Spriggs, T. Grant, et

al., (Eds.) Proceedings of the 8th ICOM Group on Wet Organic Archaeological Materials Conference, Stockholm, 2001, 67-90.

[3] M. Sandström, F. Jalilehvand, I. Persson, U. Gelius, P. Frank, I. Hall-Roth, Deterioration of the Seventeenth-century Warship Vasa by Internal Formation of Sulphuric Acid. *Nature* **415**, 2002, 893–897.

[4] H.A. Videla, W.G. Characklis, Biofouling and Microbiologically Induced Corrosion, *Int. Biodeter. Biodegr.* **29**, 1992, 195-212. https://doi.org/10.1016/0964-8305(92)90044-O.

[5] W. Lee and W.G. Characklis, Corrosion of mild steel under anaerobic biofilm. *Corrosion* **49**, 1993, 186-199, https://doi.org/10.5006/1.3316040.

[6] P. Angell, J.-S. Luo and D.C. White, Microbially sustained pitting corrosion of 304 stainless steel in anaerobic seawater. *Corros. Sci.* **37**, 1995, 1085-1096, https://doi.org/10.1016/0010-938X(95)00016-D.

[7] P. Angell, Understanding Microbially Influenced Corrosion as Biofilm-mediated Changes in Surface Chemistry. *Curr. Opin. Biotechnol.* **10**, 1999, 269-272, https://doi.org/10.1016/S0958-1669(99)80047-0.

[8] R. Marchal, Rôle des bactéries sulfurogènes dans la corrosion du fer. *Oil Gas Sci. Technol.* **54**, 1999, 649-659, https://doi.org/10.2516/ogst:1999054.

[9] I.B. Beech and J. Sunner, Biocorrosion: Towards Understanding Interactions Between Biofilms and Metals. *Curr. Opin. Biotechnol.* **15**, 2004, 181-186, https://doi.org/10.1016/j.copbio.2004.05.001.

[10] B.J. Little and J.S. Lee, 2007. Microbiologically Influenced Corrosion. Jon Wiley and sons, Inc., Hoboken, New Jersey. https://doi.org/10.1002/047011245X.

[11] D. Rickard, A. Griffith, A. Oldroyd, I.B. Butler, E. Lopez-Capel, D.A.C. Manning, D.C. Apperley,. The composition of nanoparticulate mackinawite, tetragonal iron(II) monosulfide. *Chem. Geol.* **235**, 2006, 286-298, https://doi.org/10.1016/j.chemgeo.2006.07.004.

[12] D. Rickard and G.W. Luther III, Chemistry of Iron Sulfides. *Chem. Rev.* **107**, 2007, 514-562, https://doi.org/10.1021/cr0503658.

[13] Roth, S.H., 1993, Hydrogen Sulfide, Handbook of Hazardous Materials, Academic Press, Ed. Morton Corn, 367-376, https://doi.org/10.1016/B978-0-12-189410-8.50036-5.

[14] R.T. Wilkin and H.L. Barnes, Formation processes of framboidal pyrite. *Geochim. Cosmochim. Acta* **61**, 1997, 323-339, https://doi.org/10.1016/S0016-7037(96)00320-1.

[15] L.G. Benning, R.T. Wilkin and H.L. Barnes, Reaction pathways in the Fe-S system below 100°C. *Chem. Geol.* **167**, 2000, 25-51, https://doi.org/10.1016/S0009-2541(99)00198-9.

[16] S. Hunger and L. G. Benning, Greigite: a true intermediate on the polysulfide pathway to pyrite. *Geochemical Trans*. 8, 2007, 1-20, https://doi.org/10.1186/1467-4866-8-1.

[17] J.-A. Bourdoiseau, M. Jeannin, C. Rémazeilles, R. Sabot and Ph. Refait, The transformation of mackinawite into greigite studied by Raman spectroscopy. *J Raman Spectrosc* **42**, 2011, 496-504, https://doi.org/10.1002/jrs.2729.

[18] D. Rickard, Kinetics and mechanism of the sulfidation of goethite. *Am. J. Sci.* **274**, 1974, 941-952. https://doi.org/10.2475/ajs.274.8.941.

[19] M. Dos Santos Afonso and W. Stumm, Reductive Dissolution of Iron(III) (Hydr)oxides by Hydrogen Sulfide. *Langmuir* **8**, 1992, 1671-1675, https://doi.org/10.1021/la00042a030.

[20] S.W. Poulton, Sulfide oxidation and iron dissolution kinetics during the reaction of dissolved sulfide with ferrihydrite. *Chem. Geol.* **202**, 2003, 79-94, https://doi.org/10.1016/S0009-2541(03)00237-7.

[21] S.W. Poulton, M.D. Krom and R. Raiswell, A revised scheme for the reactivity of iron (oxyhydr)oxide minerals towards dissolved sulfide. *Geochim. Cosmochim. Acta* **68**, 2004, 3703-3715, https://doi.org/10.1016/j.gca.2004.03.012.

[22] Ph. Refait, J.A. Bourdoiseau, M. Jeannin, R. Sabot, and C. Rémazeilles, Interactions between sulphide species and components of rust. In: European Federation Corrosion Series, EFC N°59, "Sulphur-assisted corrosion in nuclear disposal systems", The Institute of Materials, London, 2011, 124-136.

[23] C. Rémazeilles, D. Neff, J.A. Bourdoiseau, R. Sabot, M. Jeannin and Ph. Refait, Role of previously formed corrosion layers on sulfide-assisted corrosion of iron archaeological artefacts in soil. *Corros Sci* **129**, 2017, 169-178. https://doi.org/10.1016/j.corsci.2017.10.011

[24] C. Rémazeilles, K. Tran, E. Guilminot, E. Conforto and P. Refait, Study of Fe(II) sulfides in waterlogged archaeological wood. *Stud Conserv* **58**, 2013, 297-307, https://doi.org/10.1179/2047058412Y.0000000071.

[25] C. Rémazeilles, F. Lévêque, E. Conforto, L. Meunier and Ph. Refait, Contribution of magnetic measurement methods to the analysis of iron sulfides in archaeological waterlogged wood-iron assemblies. *Microchem. J.* **148**, 2019, 10-20, https://doi.org/10.1016/j.microc.2019.04.062.

[26] C. Rémazeilles, L. Meunier, F. Lévêque, N. Plasson, E. Conforto, M. Crouzet, Ph. Refait and L. Caillat, Post-treatment Study of Iron/Sulfur-containing Compounds in the Wreck of Lyon Saint-Georges 4 (Second Century ACE), *Stud Conserv* **65**, 2020, 28-36, https://doi.org/10.1080/00393630.2019.1610608.

[27] M.P. Jézégou, J. Cavéro, M. Druez, H. Günter-Martin, V. Mathé, C. Sanchez and K. Storch,. A geo-archaeological research about the Roman Harbours of Narbonne : earth and underwater survey and GIS, In : J. Henderson (Ed.) IKUWA 3 Beyond Boundaries, Proceedings of the 3rd International Congress on Underwater Archaeology, London 2008, 2012, 299-307.

[28] C. Sanchez, C. Faïsse, M.P. Jézégou and V. Mathé, Le système portuaire de Narbonne antique : approche géoarchéologique, In : L. Mercuri, R. González, F. Bertoncello (Eds.),

Implantations humaines en milieu littoral Méditerranéen : facteurs d'installation et processus d'appropriation de l'espace, de la Préhistoire au Moyen Âge, Actes des 24ème rencontres internationales d'archéologie et d'histoire d'Antibes, 2014, 125-136.

[29] V. Mathé, C. Sanchez, G. Bruniaux, A. Camus, J. Cavero, C. Faisse, M.-P Jézégou, J. Labussière and F. Lévêque, Prospections géophysiques multi-méthodes de structures portuaires antiques à Narbonne (Aude, France). *ArcheoSciences* **40**, 2016, 47-63, https://doi.org/10.4000/archeosciences.4732

[30] G. Ayala, Lyon. Évolution d'un bord de Saône de l'Antiquité à nos jours : la fouille du Parc Saint-Georges, Bilan préliminaire, *Rev Archeol-Est* **56**, 2007, 153-185. http://journals.openedition.org/rae/1380

[31] J. Letuppe, Premiers résultats de la fouille de l'épave antique n°2 de Courbiac (Saintes-Fontcouverte, 17100). *Bulletin de la Société d'archéologie et d'histoire de la Charente-Maritime* **43**, 2016, 147-158.

[32] Ph. Refait, M. Jeannin, R. Sabot, H. Antony and S. Pineau, Electrochemical formation and transformation of corrosion products on carbon steel under cathodic protection in seawater, *Corros Sci* **71**, 2013, 32-36, https://doi.org/10.1016/j.corsci.2013.01.042.

[33] Ph. Refait, A.-M. Grolleau, M. Jeannin, E. François and R. Sabot, Localized corrosion of carbon steel in marine media: galvanic coupling and heterogeneity of the corrosion product layer, *Corros Sci* **111**, 2016, 583-595, https://doi.org/10.1016/j.corsci.2016.05.043

[34] Ph. Refait, A.-M. Grolleau, M. Jeannin, E. François and R. Sabot, Corrosion of carbon steel at the mud zone/seawater interface: mechanisms and kinetics, *Corros Sci* **130**, 2018, 76-84, https://doi.org/10.1016/j.corsci.2017.10.016.

[35] Ph. Refait, M. Jeannin, E. François, R. Sabot and A.-M. Grolleau, Galvanic corrosion in marine environments: effects associated with the inversion of polarity of Zn / carbon steel couples, *Werkst. Korros.* **70**, 2019, 950-961, https://doi.org/10.1002/maco.201810568.

[36] P. Murkute, S. Pasebani, O. Burgan Isgor, Metallurgical and Electrochemical Properties of Super Duplex Stainless Steel Clads on Low Carbon Steel Substrate produced with Laser Powder Bed Fusion, *Sci. Rep*. 10**:**10162**,** 2020, https://doi.org/10.1038/s41598-020-67249-2.

[37] H. Dong, Y. Zhang, G. Miyamoto, H. Chen, Z. Yang, T. Furuhara, A comparative study on intrinsic mobility of incoherent and semicoherent interfaces during the austenite to ferrite transformation, *Scr. Mater.* **188**, 2020, 59–63, https://doi-org.gutenberg.univ-lr.fr/10.1016/j.scriptamat.2020.07.007.

[38] M. Reffass, R. Sabot, C. Savall, M. Jeannin, J. Creus and Ph. Refait, Localised corrosion of carbon steel in NaHCO3/NaCl electrolytes: Role of Fe(II)-containing compounds, *Corros Sci* **48**, 2006, 709-726, https://doi.org/10.1016/j.corsci.2005.02.016.

[39] I. Azoulay, C. Rémazeilles and Ph. Refait, Corrosion of steel in carbonated media: the oxidation processes of chukanovite ($Fe_2(OH)_2CO_3$), *Corros Sci* **85**, 2014, 101-108, https://doi.org/10.1016/j.corsci.2014.04.004.

[40] I. Azoulay, C. Rémazeilles, Ph. Refait, Oxidation of chukanovite ($Fe_2(OH)_2CO_3$): Influence of the concentration ratios of reactants, *Corros Sci* **98**, 2015, 634-642, https://doi.org/10.1016/j.corsci.2015.06.002.

[41] S. Réguer, P. Dillmann and F. Mirambet, Buried iron archaeological artefacts: Corrosion mechanisms related to the presence of Cl-containing phases, *Corros Sci* **49**, 2007, 2726–2744, https://doi.org/10.1016/j.corsci.2006.11.009.

[42] J.-A. Bourdoiseau, M. Jeannin, R. Sabot, C. Rémazeilles and Ph. Refait, Characterisation of mackinawite by Raman spectroscopy: Effects of crystallisation, drying and oxidation. *Corros Sci* **50**, 2008, 3247–3255, https://doi.org/10.1016/j.corsci.2008.08.041.

[43] W. Davison, The solubility of iron sulphides in synthetic and natural waters at ambient temperature. *Aquat Sci* **53**, 1991, 309-329, https://doi.org/10.1007/BF00877139.

[44] D. Rickard, The solubility of FeS. *Geochim. Cosmochim. Acta* **70**, 2006, 5779-5789, https://doi.org/10.1016/j.gca.2006.02.029.

[45] M. Mullet, S. Boursiquot, M. Abdelmoula, J.-M. Génin, J.-J. Ehrhardt, Surface chemistry and structural properties of mackinawite prepared by reaction of sulfide ions with metallic iron, *Geochim. Cosmochim. Acta* **66,** 2002, 829-836, https://doi.org/10.1016/S0016-7037(01)00805-5.

[46] A.R. Lennie, S.A.T. Redfern, P.E. Champness, C.P. Stoddart, P.F. Schofield, D.J. Vaughan, Transformation of mackinawite to greigite: An in situ X-ray powder diffraction and transmission electron microscope study, *Am. Mineral.* **82,** 1997**,** 302-309, https://doi.org/10.2138/am-1997-3-408

[47] S. Grousset, M. Bayle, A. Dauzeres, D. Crusset, V. Deydier, Y. Linnard, P. Dillmann, F. Mercier-Bion, D. Neff, Study of iron sulphides in long-term iron corrosion, processes: Characterisations of archaeological artefacts. *Corros Sci* **112**, 2016, 264-275, https://doi.org/10.1016/j.corsci.2016.07.022.

Figure captions

Figure 1. Hull timber fragment extracted from the wreck n°2 Courbiac-Saintes-Fontcouverte. The wood samples were cut around the nail indicated by the white arrow. The black arrow indicates the analyzed nail.

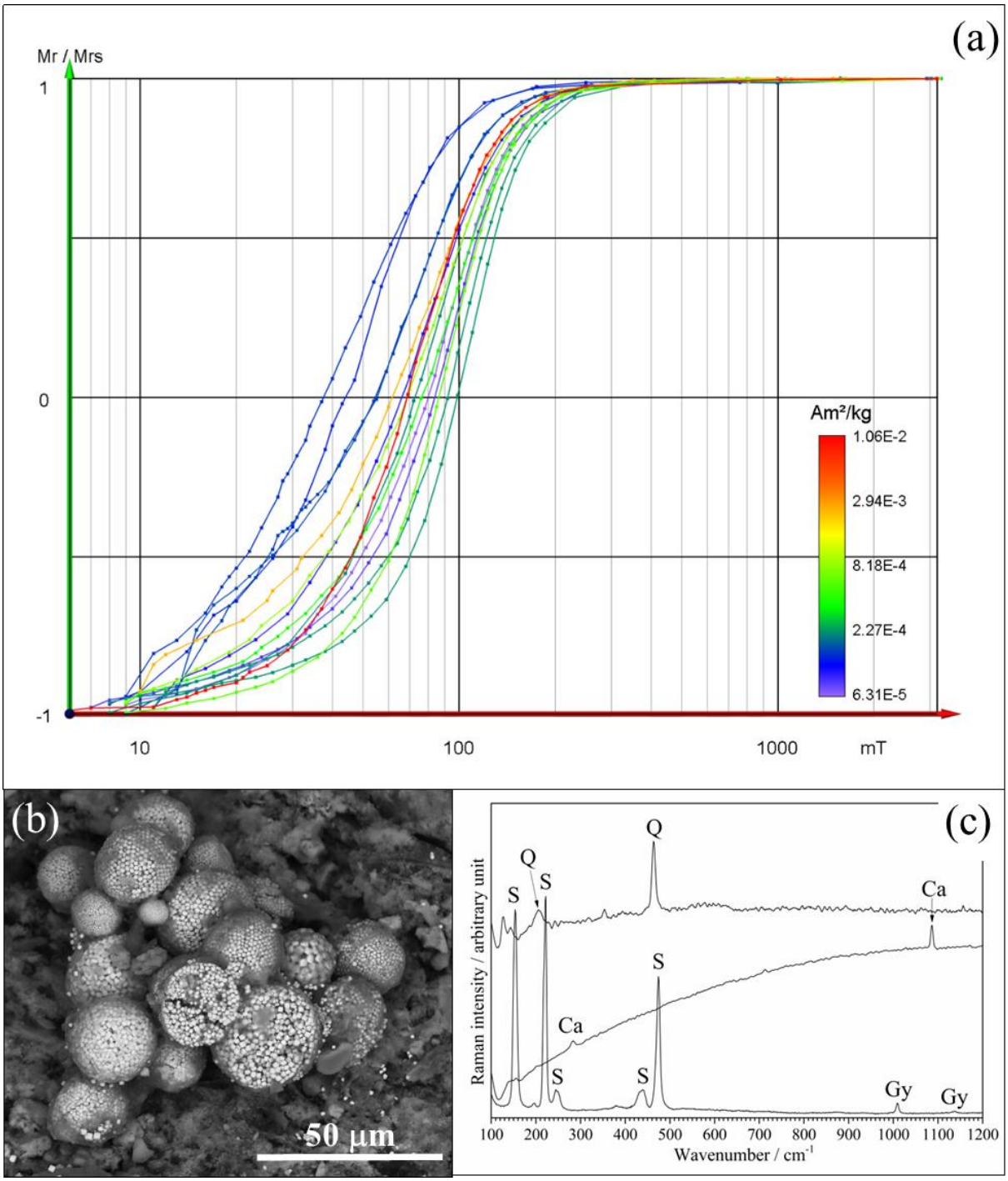

Figure 2. (a) Backfield IRM curves acquired from wooden cubes cut around the nail marked by the white arrow on Fig.1. (b) ESEM micrograph of pyrite microcrystals observed in the wood (chemical contrast). (c) Micro-Raman spectra acquired in the wood showing α-S_8 (S), gypsum (Gy), calcite (Ca) and quartz (Q).

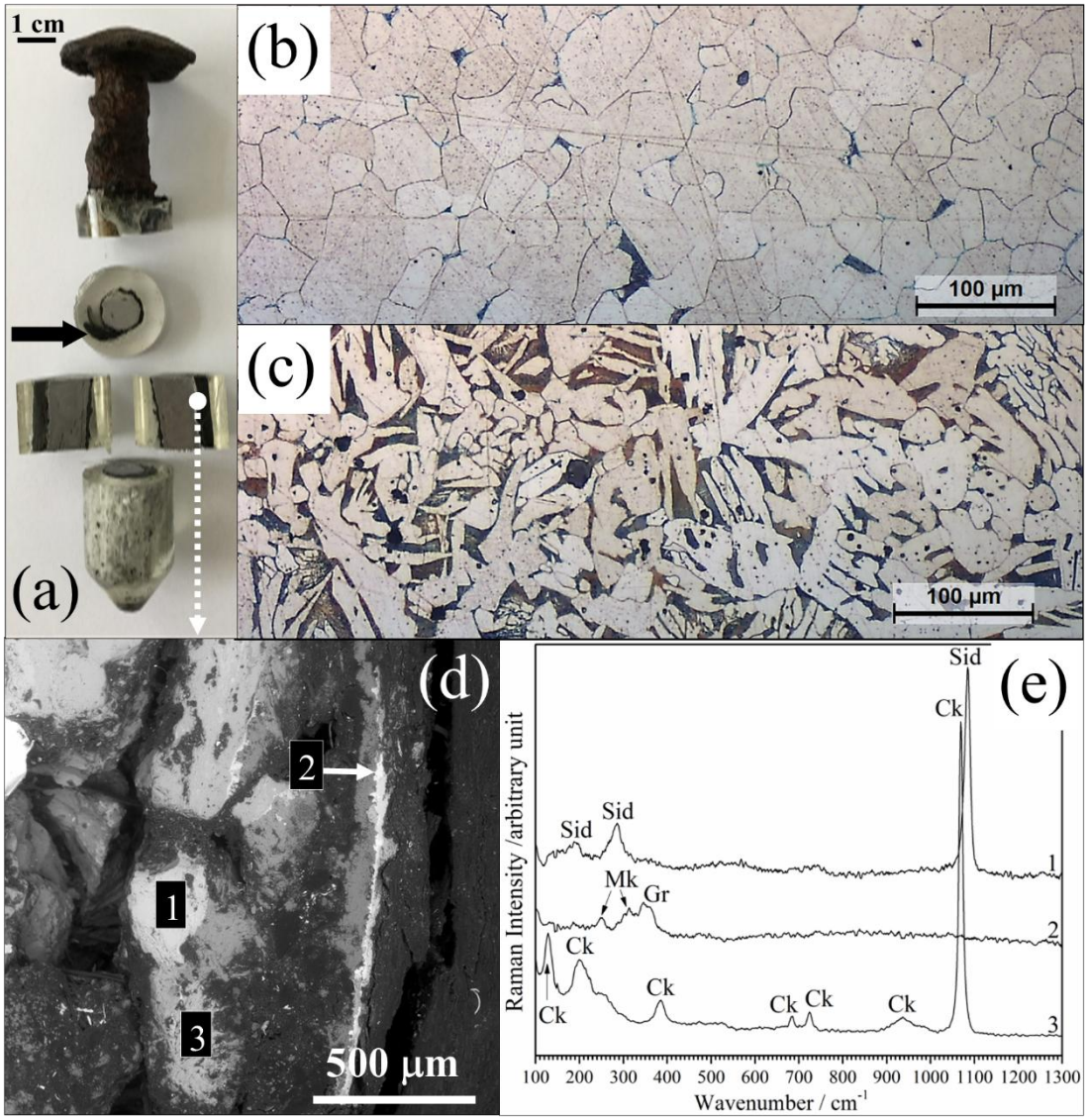

Figure 3. Analyzed nail from the wreck n°2 Courbiac-Saintes-Fontcouverte. (a) General picture. The black arrow indicates the wooden peg the nail was embedded in. (b,c) optical micrographs of the metal after a Nital (3%) attack. (d) ESEM micrograph of the corrosion layer cross section (chemical contrast). (e) Micro-Raman spectra of corrosion products labeled 1, 2, 3 in (d). Sid = siderite, Ck = chukanovite, Mk = mackinawite, Gr = greigite.

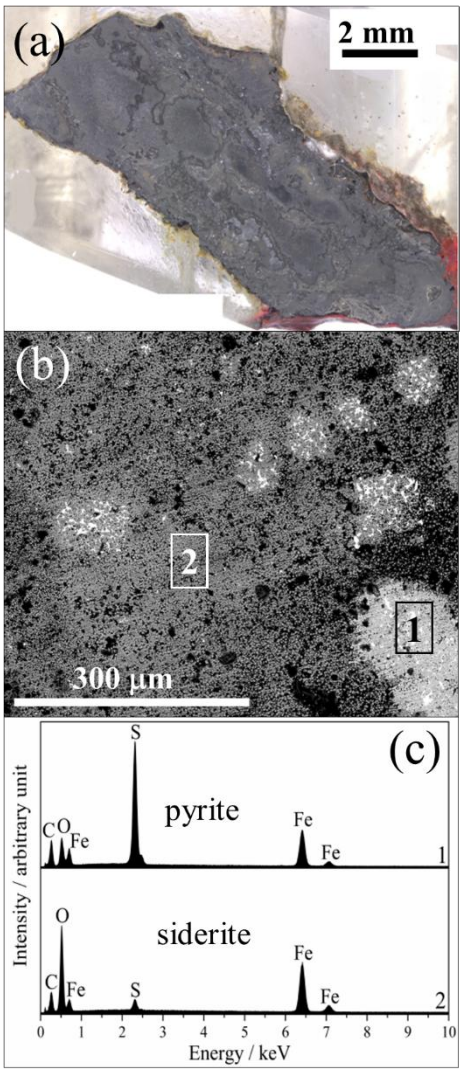

Figure 4. (a) Optical micrograph, (b) ESEM micrograph (chemical contrast) and (c) EDS spectra of the nail extracted from the wreck of Mandirac. Labels 1 and 2 correspond to acquisition areas of the EDS spectra and corresponding corrosion products.

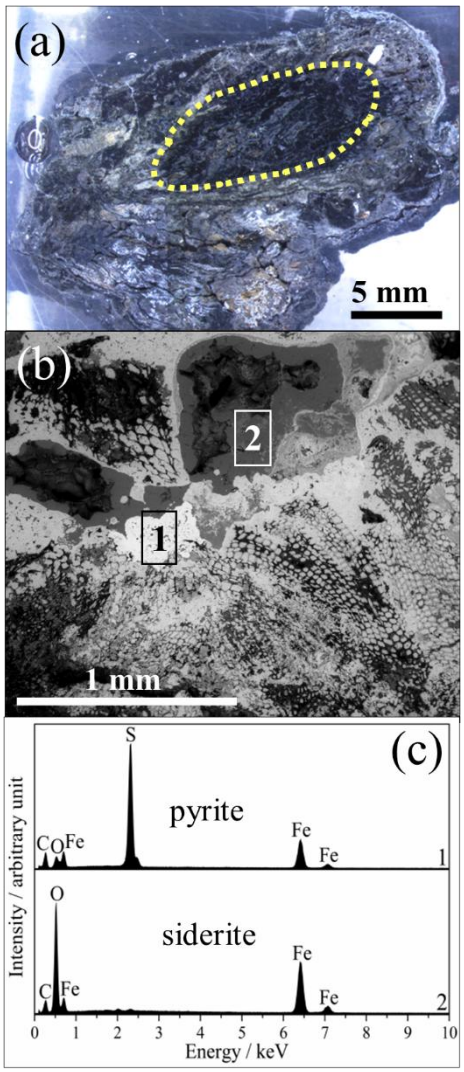

Figure 5. (a) Optical micrograph, the dashes delimitate the assumed rest of metallic core, (b) ESEM micrograph (chemical contrast) and (c) EDS spectra of the nail extracted from the wreck LSG4. Labels 1 and 2 correspond to acquisition areas of the EDS spectra and corresponding corrosion products.

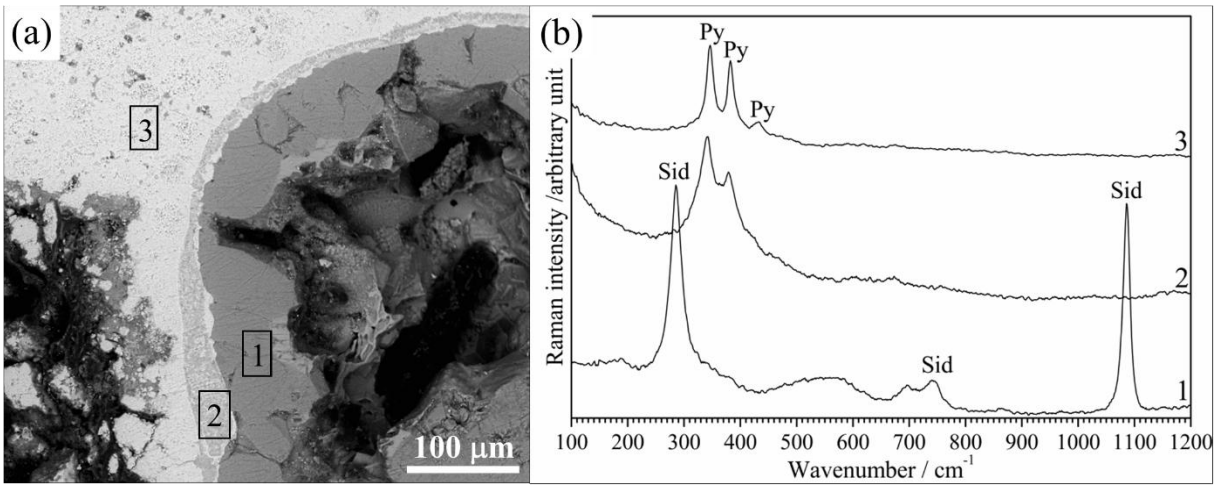

Figure 6. (a) ESEM micrograph (chemical contrast) of a detail of the cross-section of the nail from LSG4. (b) Corresponding micro-Raman spectra acquired in areas labeled 1, 2, 3. Sid = siderite, Py = pyrite.

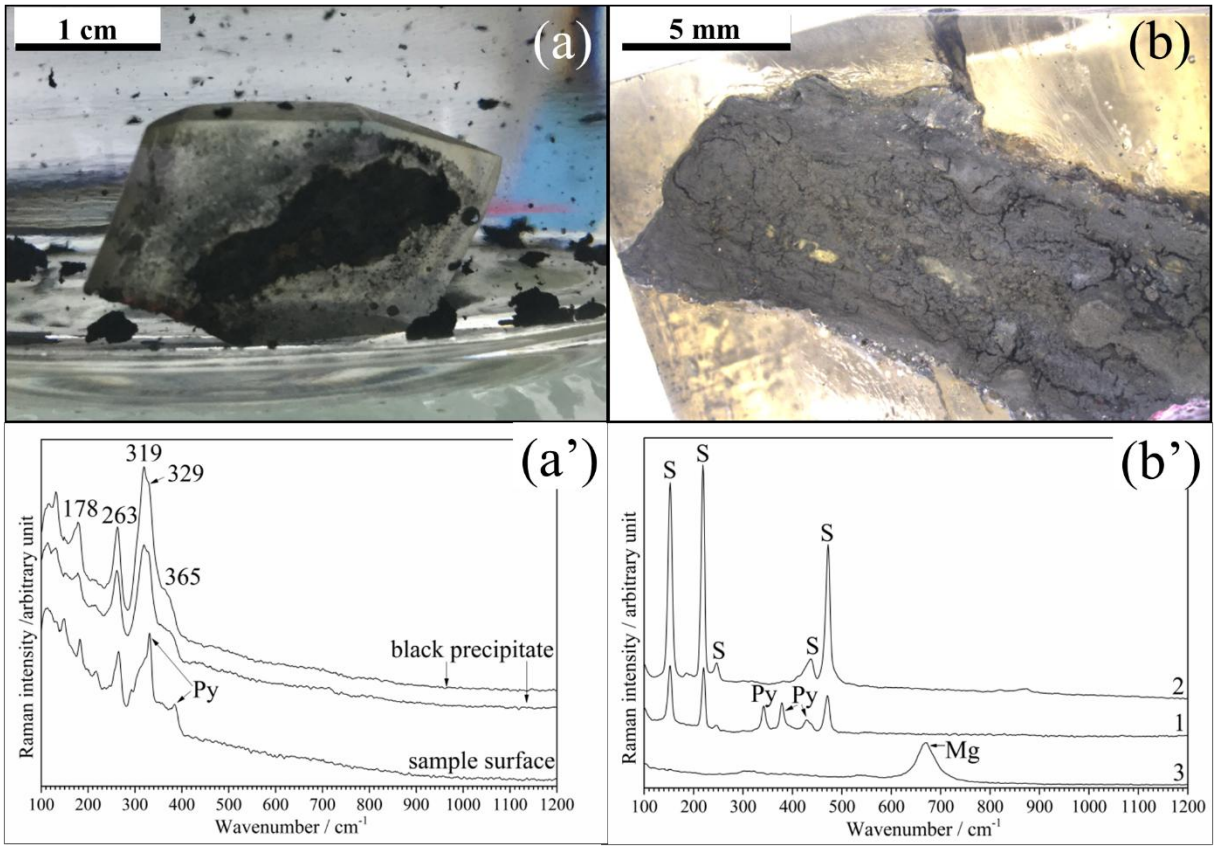

Figure 7. (a) Picture and (b) optical micrograph of both half-nails of the wreck of Mandirac and (a',b') micro-Raman spectra obtained after immersion in a neutral (a,a') and an acidic (b,b') sulfide-containing solutions. Py = pyrite, S = α-S_8, Mg = magnetite. Spectra 1, 2, 3: see in the text.

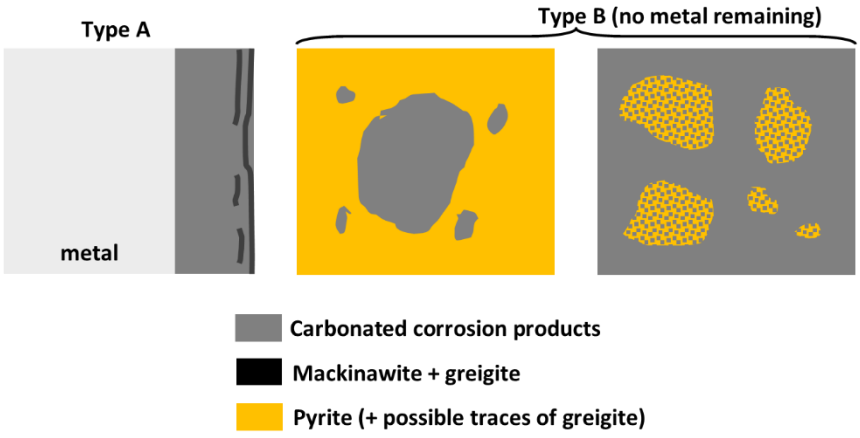

Figure 8. Schematic representation of the corrosion patterns determined from the studied reinforcements. Type A = weakly corroded artefact. Type B = highly corroded artefact.

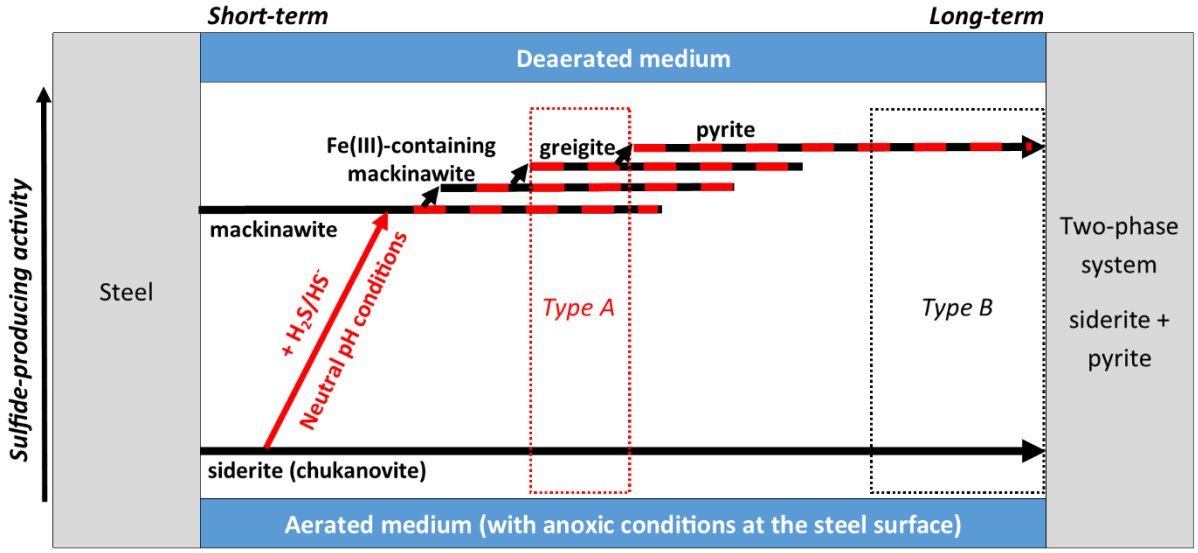

Figure 9. Schematic representation of long-term sulfide influenced evolution processes of iron alteration products in a waterlogged media.